THE INFLUENCE OF THE GRAIN BOUNDARY PHASE TRANSITIONS ON THE PROPERTIES OF NANOSTRUCTURED MATERIALS

B.B. STRAUMAL
Institute of Solid State Physics, Russian Academy of Sciences
Chernogolovka, Moscow distr., 142432 Russia

Abstract Grain boundary (GB) phase transitions can change drastically the properties of nanograined polycrystals, leading to enhanced plasticity or brittleness, increasing diffusion permeability. They influence also liquid-phase and activated sintering, soldering, processing of semi-solid materials. The GB wetting phase transition can occur in the two-phase area of the bulk phase diagram where the liquid (L) and solid (S) phases are in equlibrium. The GB wetting tie line appears in the L+S area. Above the temperature of the GB wetting phase transition a GB cannot exist in equlibrium contact with the liquid phase. The liquid phase has to substitute the GB and to separate both grains. The GB wetting tie-line can continue in the one-phase area of the bulk phase diagram as a GB solidus line. This line represents the GB premelting or prewetting phase transitions. The GB properties change drastically when GB solidus line is crossed by a change in the temperature or concentration. In case if two solid phase are in equilibrium, the GB "solid state wetting" (or covering) can occur. In this case the layer of the solid phase *2* has to substitute GBs in the solid phase *1*. Such covering GB phase transition occurs if the energy of two interphase boundaries between phase *1* and *2* is lower than the GB energy in the phase *1*.

1. Introduction

The properties of modern materials, especially those of nanocrystalline, superplastic or composite materials, depend critically on the properties of internal interfaces such as grain boundaries (GBs) and interphase boundaries (IBs). All processes which can change the properties of GBs and IBs affect drastically the behaviour of polycrystalline metals and ceramics [1]. GB phase transitions are one of the important examples of such processes [2]. Recently, the lines of GB phase transitions began to appear in the traditional bulk phase diagrams [2- 7]. The addition of these equilibrium lines to the bulk phase diagrams ensures an adequate description of polycrystalline materials, particularly their diffusion permeability, deformation behavior and the evolution of the

T. Tsakalakos, et al. (eds.) pgs. 295 - 312
Nanostructures: Synthesis, Functional Properties and Applications;

microstructure. In this work the following GB phase transitions are discussed: (a) GB wetting, (b) GB prewetting (or premelting) and (c) GB «wetting» (covering) by second solid phase. The recently obtained experimental data are discussed. Using these data, the new GB lines in the conventional bulk phase diagrams are constructed.

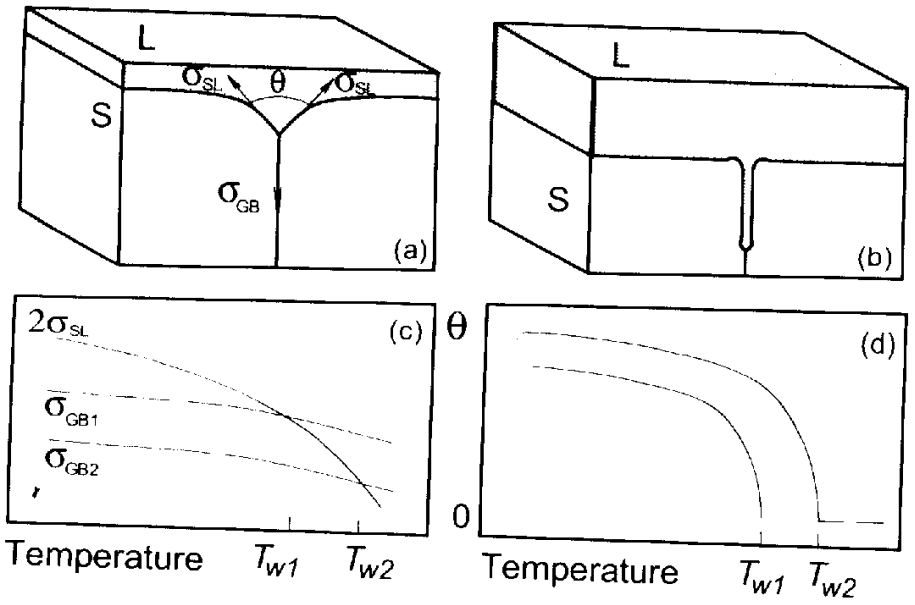

Figure 1. (a) Scheme of the equilibrium contact between the grain boundary in the solid phase *S* and the liquid phase *L* (incomplete wetting). (b) Complete GB wetting. (c) Scheme of the temperature dependence for the GB energy σ_{GB} (for two different GBs) and the energy of the solid-liquid interface boundary σ_{SL}. (d) Scheme of the temperature dependence of the contact angle θ for two grain boundaries with energies σ_{GB1} and σ_{GB2}. T_{w1} and T_{w2} are the temperatures of the GB wetting phase transition.

2. Grain Boundary Wetting Phase Transitions

In this work GB wetting, prewetting and premelting phase transitions are considered. The GB melting, GB faceting transition and the "special GB - random GB phase transitions" are analyzed elsewhere [8–10]. One of the most important GB phase transitions is the *GB wetting transition*. Since their prediction by Cahn [11] the study of wetting phase transitions has been of great experimental and theoretical interest, primarily for planar solid substrates and fluid mixtures [12–14]. Particularly, it was experimentally shown that the wetting transition is of first order, namely the discontinuity of the surface energy was measured and the hysteresis of the wetting behavior was observed [15, 16]. The important difference is that in case of GB wetting only two phases coexist, namely the liquid (melt) phase and the solid one containing the boundary between the misoriented grains. Therefore, the contact angle θ also depends only on two different surface energies (the GB energy σ_{GB} and the energy of the solid/liquid interphase boundary σ_{SL}) instead of three ones in the

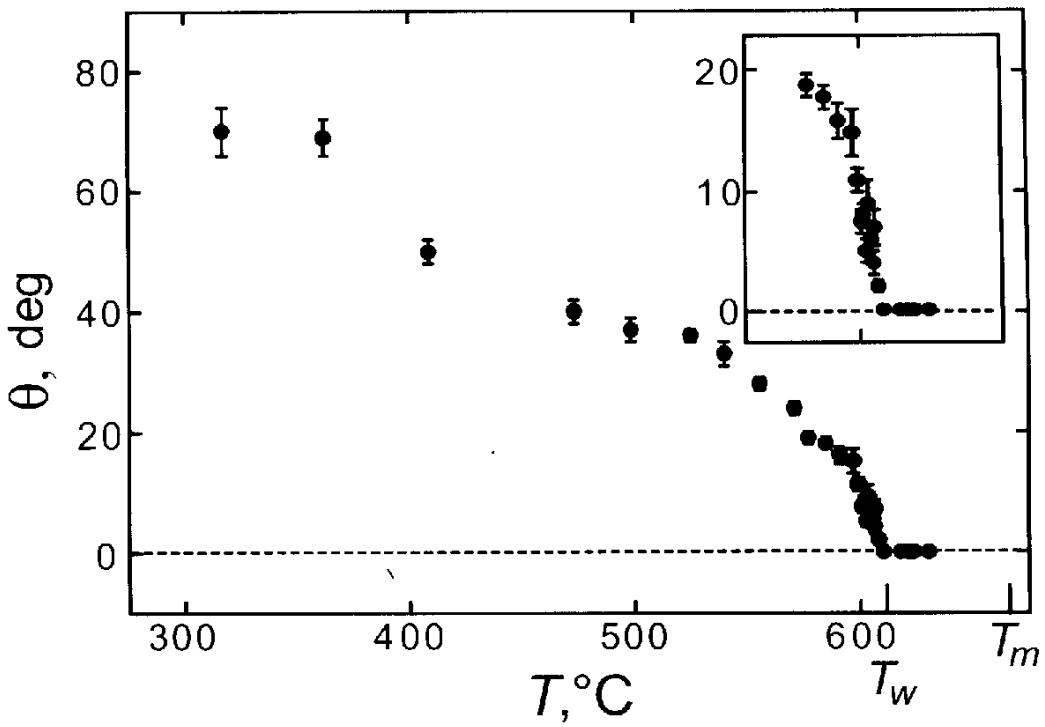

Figure 2. Temperature dependences of the contact angle between Sn-rich melt and tilt Al GB 32°<011>{001}. (T_w = 604±1°C). The insert shows the in details the $\theta(T)$ dependence close to T_w.

usual experiments: $\sigma_{GB} = 2\,\sigma_{SL}\cos(\theta/2)$. If $\sigma_{GB} < 2\sigma_{SL}$, the GB is incompletely wetted and the contact angle $\theta>0$ (Fig. 1a). At the temperature T_w of the *GB wetting phase transition* $\sigma_{GB} = 2\sigma_{SL}$ and at $T \geq T_w$ the GB is completely wetted by the liquid phase and $\theta = 0$ (Fig. 1b). If two GBs have different energies the temperatures of their GB wetting transitions will also differ: the lower σ_{GB}, the higher T_w (Figs. 1c and 1d). If the GB wetting phase transition is of first order, there is a discontinuity in the temperature derivative of the GB energy at T_w which is equal to $[\partial\sigma_{GB}/\partial T - \partial(2\sigma_{SL})/\partial T\,]$ [11, 16]. If the GB wetting phase transition is of second order, $\partial\sigma_{GB}/\partial T = \partial(2\sigma_{SL})/\partial T$ at T_w. The theory predicts also the shape of the temperature dependence $\theta(T)$ at $T \rightarrow T_w$: it must be convex for a first order wetting transition [$\theta \sim \tau^{1/2}$ where $\tau = (T_w - T)/T_w$] and concave for a second order wetting transition: $\theta \sim \tau^{3/2}$ [12].

Nowdays, the GB phase transitions of the second order were not observed experimentally. All observed temperature dependences $\theta(T)$ have a discontinuity in the temperature derivative of the GB energy at T_w. The $\theta(T)$ dependences are convex (like those shown in Fig. 2 for the Al–Sn system) and follow the $\theta \sim \tau^{1/2}$ law [17].

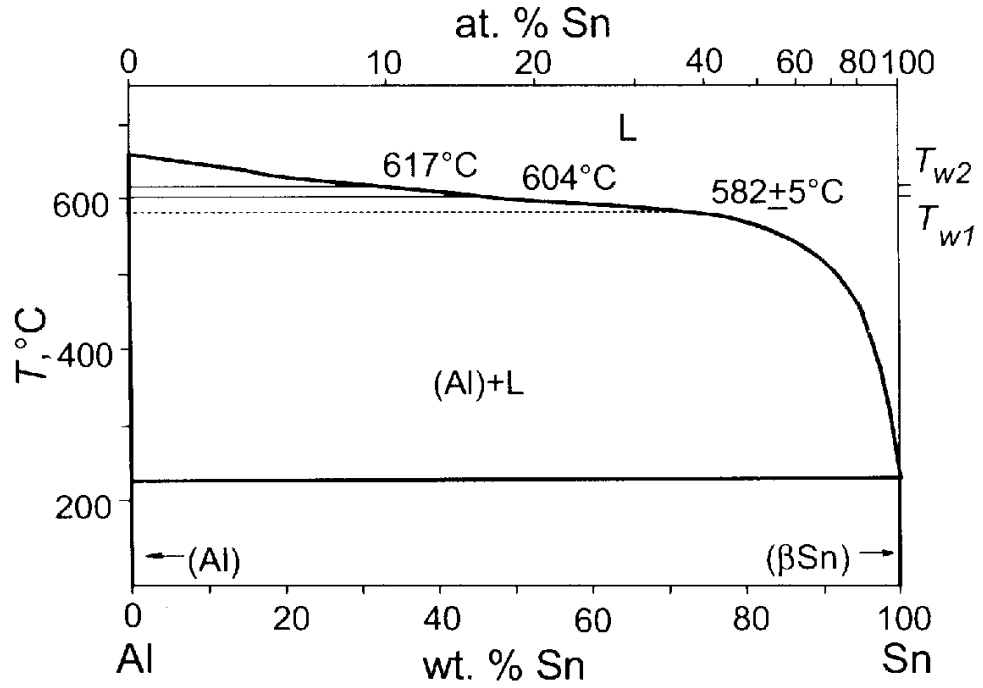

Figure 3. The Al–Sn phase diagram. Thick solid lines represent the bulk phase transitions. Thin solid lines are the tie lines of the GB wetting phase transitions. Thin dotted line represents the estimation for the GB wetting phase transiton for the GB with highest possible energy.

Consider the contact between a bicrystal and a liquid phase L. If the GB energy σ_{GB} is lower than the energy of two solid/liquid interfaces $2\sigma_{SL}$, the GB is not completely wetted and the contact angle $\theta > 0$ (Fig. 1a). If $\sigma_{GB} > 2\sigma_{SL}$ the GB is wetted completely by the liquid phase and $\theta = 0$ (Fig. 1b). If the temperature dependences σ_{GB} (T) and $2\sigma_{SL}$ (T) intersect, then the GB wetting phase transition proceeds at the temperature T_w of their intersection (Fig. 1c). The contact angle θdecreases gradually with increasing temperature down to zero at T_w. (see also the Fig. 2 for the system Cu–In) At $T > T_w$ the contact angle $\theta = 0$ (Figs. 1d and 2). The *tie-line of the GB wetting phase transition* appears at T_w in the two-phase region ($S + L$) of the bulk phase diagram (Fig. 3). Above this tie line GBs with an energy σ_{GB} cannot exist in equilibrium with the liquid phase. The liquid phase forms a layer separating the crystals. In Fig. 3 two GB wetting tie lines are shown for two GBs with different energies obtained by measurements of $\theta(T)$ dependences (Fig. 2). In polycrystals the whole spectrum of GBs exist with varuious energies. Therefore, in polycrystals the maximal T_{wmax} and minimal T_{wmin} can be found for high-angle GBs with minimal and

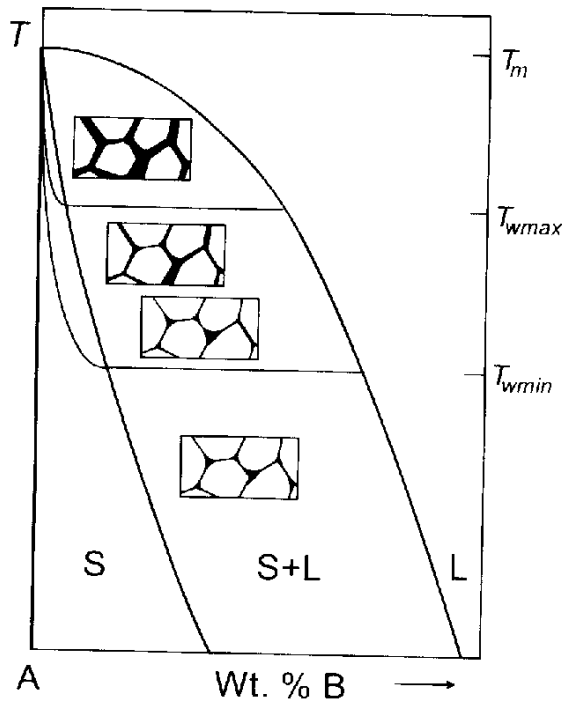

Figure 4. Scheme of the phase diagram with lines of bulk and GB phase transitions. Thick lines represent the bulk phase transitions. Thin lines represent the tie-lines of the GB wetting phase transition in the $S + L$ area for the high angle GBs having maximal and minimal possible energy and the GB premelting phase transition in the solid solution area S.

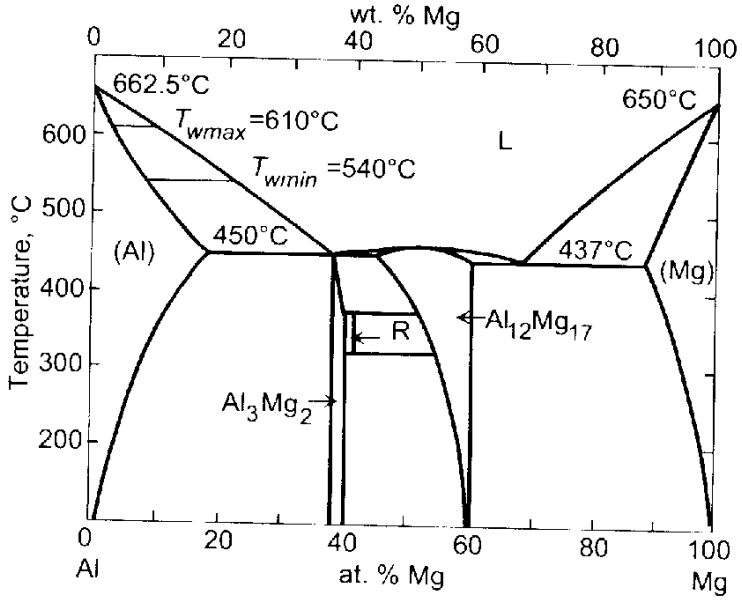

Figure 5. The Al–Mg phase diagram. Thick lines represent the bulk phase transitions. Thin lines are the tie-lines of the GB wetting phase transitions (T_{wmax} = 610°C and T_{wmin} = 540°C)

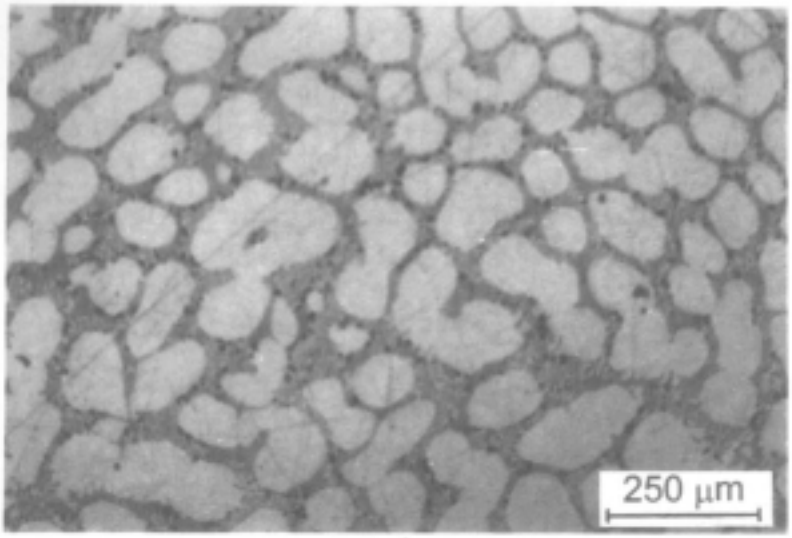

Figure 6.
Microstructure of Al – 10 wt.% Mg polycrystals in two phase *S+L* area of Al – Mg phase diagram

(a) 610°C, all GBs are wetted by the melt

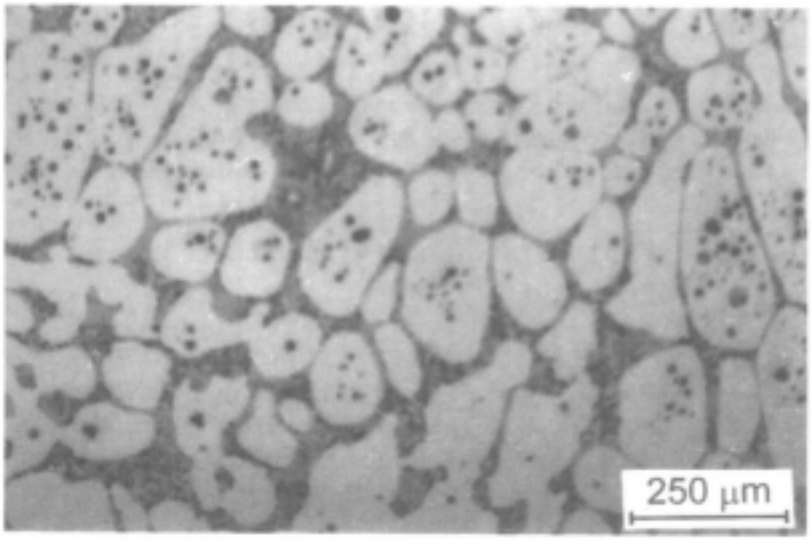

(b) 581°C, some GBs are wetted by the melt, another GBs are not wetted

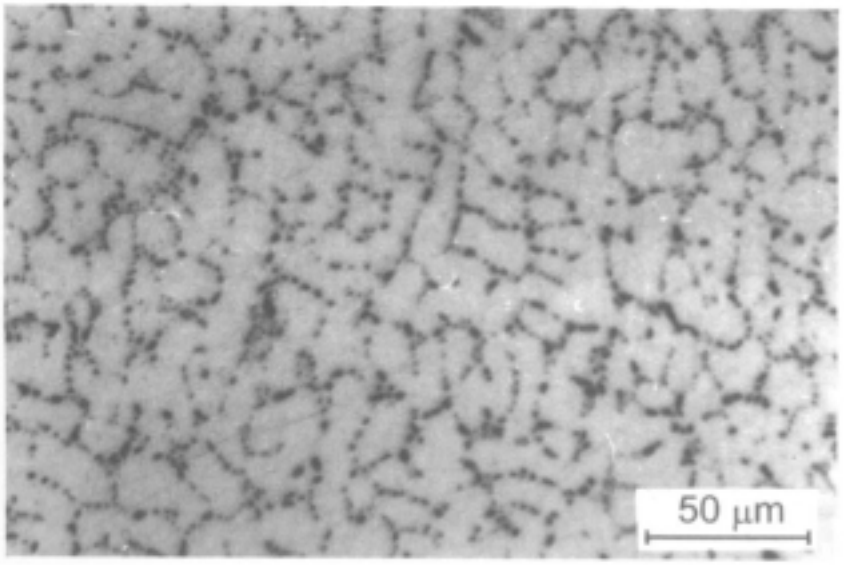

(c) 490°C, no wetted GBs in polycrystal

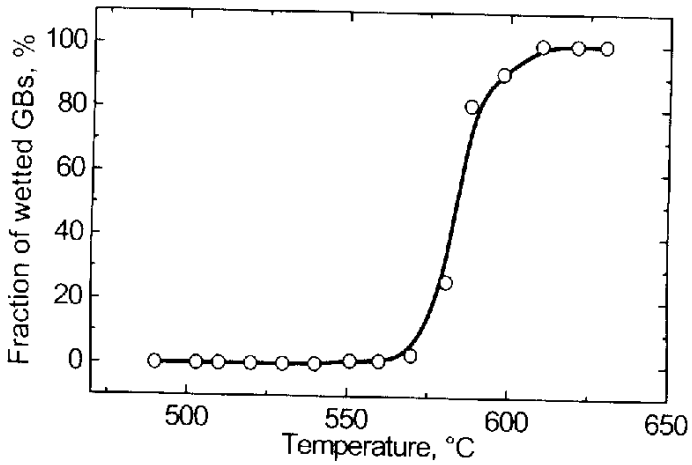

Figure 7...Temperature dependence of the fraction of wetted GBs in two-phase Al Mg polycrystals.

maximal energy σ_{GBmin} and σ_{GBmax}, respectively (Fig. 4). The tie-lines at T_{wmax} and T_{wmin} are shown also in the Al–Mg phase diagram (Fig. 5). Above T_{wmax}, all GBs are completely wetted (see Fig. 6a). At the temperature between T_{wmax} and T_{wmin} some GBs are wetted by the liquid phase and other GBs are not wetted (Fig. 6b). Below T_{wmin} all GBs are not wetted, and the melt has a shape of separated inclusions (Fig. 6c). With increasing temperature between and the fraction of the wetted GBs increases from 0 at T_{wmin} to 100% at T_{wmax} (Fig. 7).

First indications of the GB wetting phase transitions were found by measuring of the contact angles in polycrystals [17]. Correct measurements were later perfomed using metallic bicrystals with inndividual tilt GBs in the Al–Sn (Figs. 2 and 3), Cu–In [4], Al–Pb–Sn [3,18,19], Al–Ga, Al–Sn–Ga [20, 21], Cu–Bi [5, 22, 23, 30], Fe–Si–Zn [24–27], Mo–Ni [28], W–Ni [29] and Zn–Sn [7] systems. The tie-lines of the GB wetting phase transition were constructed basing on the experimental data [3, 4, 7, 18–29]. The difference in the GB wetting phase transition temperature was experimentally revealed for GBs with different energies [4, 18]. The precize measurements of the temperature dependence of the contact angle revealed also that the GB wetting phase transition is of the first order [18]. The indications of presence of the liquid-like phase along the dislocation lines were also found [23].

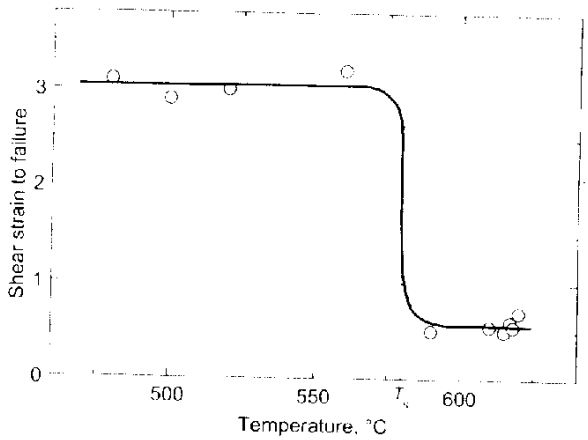

Figure 8..Temperature depen-dence of shear strain to failure for Al 5 wt. % Mg alloy in solid and semi-solid state [37].

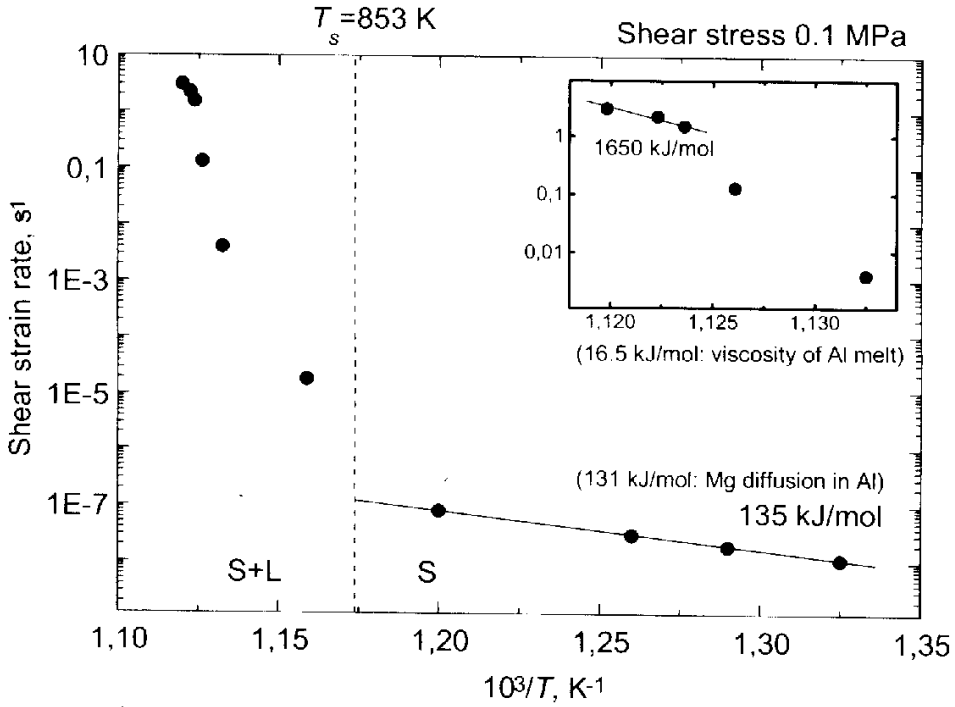

Figure 9. Temperature dependence of shear strain rate for Al–5 wt. % Mg alloy in solid and semi-solid state [37].

The deformation behavior of metals in the semi solid state has been extensively investigated from the viewpoint of rheological flow [30–32]. These studies have shown that the viscosity of the semi-solid metals depends on the volume fraction and morphology of the solid phase and the shear strain rate. In addition, the deformation behavior in a semi-solid state at the early stages of melting has been investigated by compressive creep tests [33–36]. Vaandrager and Pharr [24] showed that the deformation mechanism in a semi-solid state at the early stages of melting is grain boundary sliding accommodated by cavitation in a liquid phase for the copper containing a liquid bismuth. This deformation mechanism in the semi-solid state at the early stages of melting appears to be different from that in the semi-solid state during solidification. The presence of a liquid phase gives rise to complicated effects on the deformation behavior in the semi-solid state. Deformation in the semi-solid state is phenomenologically divided as follows: plastic deformation of solid phases, sliding between solid phases, flow of liquid incorporating solid phases and liquid flow [22]. For compressive deformation, because the liquid phase is squeezed out of boundaries experiencing compressive stresses in a very short time [24], it is difficult to investigate deformation related to the liquid flow by compressive tests. In [37] the shear tests were carried out over a wide temperature range of 480–620°C, including temperatures below and above the solidus temperature, for Al – 5 wt.% Mg alloy to investigate deformation behavior in semi-solid states at early stages of melting. Pharr et al. [36] showed that the liquid phase significantly affects creep behavior of alloys when a significant portion of the grain boundary area, in excess of 70%, is wet. This revealed that the volume fraction of the liquid phase is an important factor in the deformation characteristics in the semi-solid state. The same trend has been reported in a semi-solid state at

solidification [34]. However, deformation in the semi-solid state is very complicated and cannot be characterized only by the volume fraction of a liquid phase. In [37] the pure shear of Al 5 wt% Mg alloy was investigated. This method permits to exclude the squeezing of the liquid phase from the sample. The shear strain to failure drops drastically at the solidus temperature (Fig. 8) [37]. In the semi-solid phase it is about 6 times lower than in the solid solution. Using the micrographs of the structure of polycrystals in the semi-solid state from [37] we calculated the fraction of the fully wetted GBs in dependence on the temperature. This dependence is shown in the Fig. 7. The continuous change of the fraction of wetted GBs influences strongly the mechanism of the deformation. In Fig. 9 the temperature dependence of the shear strain rate is shown recalculated from the data [37]. In the solid solution the of the shear strain rate increases moderately with increasing temperature, and the activation energy (135 kJ/mol) is very close to the activation energy of Mg diffusion in Al (131 kJ/mol). In the semi-solid state the shear strain rate increases drastically. Close to T_{wmax} the (formally calculated) activation energy is about 1650 kJ/mol, i.e. ten times higher than the activation energy for the viscosity of Al melt. It means that in the semi-solid state no unique thermally activated mechanism is working. Due to the temperature increase of the fraction of wetted GBs, the structure of the solid skeleton changes continuously. It becomes more and more cutted with increasing temperature, therefore, making the shear easier in addition to the pure temperature activation.

3. Grain Boundary Prewetting (Premelting) Phase Transitions

It was pointed out by Cahn [38] that, when the critical consolution point of two phases is approached, GBs of one critical phase should be wetted by a layer of another critical phase, and in the one-phase region of a phase diagram there should be a singularity connected with an abrupt transition to a microscopic wetting layer. We distinguish two possible situations: the first one, when a layer of the new phase is formed on the GB (*prewetting transition*), and the second one, when the GB is replaced by a layer of the new phase (*premelting phase transition*). At the prewetting transition the difference between two phases must be small, while at the premelting transition the wetting phase may differ from that of the bulk dramatically. The lines of the GB prewetting or premelting phase transitions appear in the one-phase areas of the bulk phase diagrams where only one bulk phase can exist in the thermodynamic equilibrium (e.g. solid solution S, see Fig. 4). These lines continue the tie-lines of the GB wetting phase transitions and represent the GB solidus (Fig. 4). The thin liquid-like layer of the GB phase exists on the GBs between the bulk solidus and GB solidus in the phase diagram. During the GB premelting phase transition this layer appears abruptly on the GB by the intersection of GB solidus. As a result, the GB properties (diffusivity, mobility, segregation) change dramatically.

In other words, above the GB wetting tie line T_W in the $S+L$ area of the bulk phase diagram $\sigma_{GB} > 2\sigma_{SL}$. This is true also if we intersect the bulk solidus at T = const and move into the one-phase area S of the bulk phase diagram. The GB energy σ_{GB} in this part of the one-phase region is still higher that the energy $2\sigma_{SL}$ of two solid-liquid

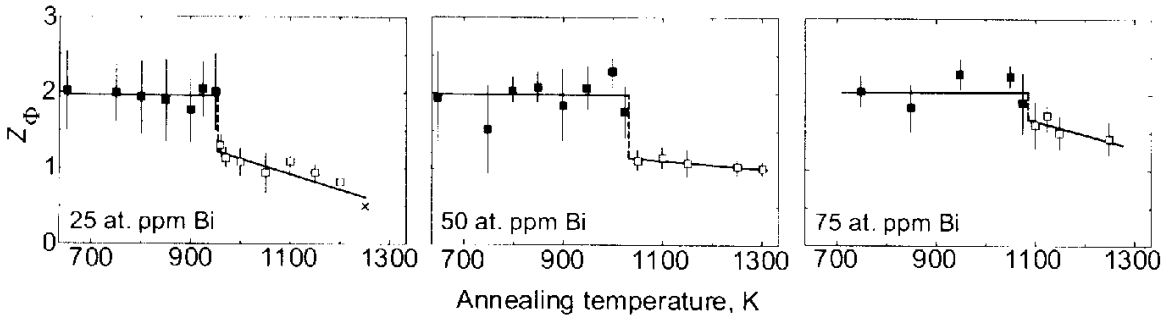

Figure 10. Temperature dependence of the GB Gibbsian excess of Bi in Cu(Bi) polycrystals of various compositions, measured by AES. The sudden change of the GB segregation corresponds to the intersection of GB solidus line.

interphase boundaries. Therefore, the GB still can be substituted by two solid-liquid interfaces, and the energy gain $G = \sigma_{GB} - 2\sigma_{SL}$ appears by this substitution. G permits to stabilize the GB layer of the liquid-like phase. The appearance of the liquid-like phase (otherwise unstable in the bulk) between two *S/L* interfaces instead of GB leads to the energy loss g per unit thickness and unit square. Therefore, the GB layer of the liquid-like phase has the thickness l defined by the equation $\sigma_{GB} - 2\sigma_{SL} = \Delta g l$. Thickness l depends on the concentration and temperature and becomes $l = 0$ at the line of GB premelting (or prewetting) phase transition.

The premelting transition has been revealed in the ternary Fe–Si–Zn system by measurements of Zn GB *diffusivity* along tilt GBs in the Fe–Si alloys [24–27]. It was found that the penetration profiles of Zn along GBs consist of two sections, one with a small slope (high GB diffusivity $D_b\delta$) at high Zn concentrations and one with a large slope (low GB diffusivity) at low Zn concentrations. The transition from one type of behavior to the other was found to occur at a definite Zn concentration c_{bl} at the GB, which is an equilibrium characteristic of a GB and depends on the temperature and pressure. The GB diffusivity increases about two orders of magnitude which is an indication of a quasi-liquid layer present in the GBs at high Zn concentration. The line of GB premelting phase transition in the one-phase area of the bulk phase diagram continues the line of the GB wetting phase transition in the two-phase $L+S$ area: by pressure increase both the GB wetting and the GB enhanced diffusivity disappear together at the same pressure value [27].

The *GB mobility* was studied for two tilt GBs in bicrystals grown of high purity 99.999 wt.% Al and of the same material doped by 50 wt. ppm Ga [21]. The GB mobility increased about 10 times by addition of the Ga content for the both GBs studied. Normally, the addition of a second component can only decrease the GB mobility due to the solution drag [32]. The increase of the GB mobility can only be explained by the formation of the liquid-like Ga-rich layer on the GBs as a result of a premelting phase transition

The *GB segregation* of Bi in Cu was studied in the broad temperature and concentration interval [5, 22, 23, 39, 40]. It was shown that at a fixed Bi concentration

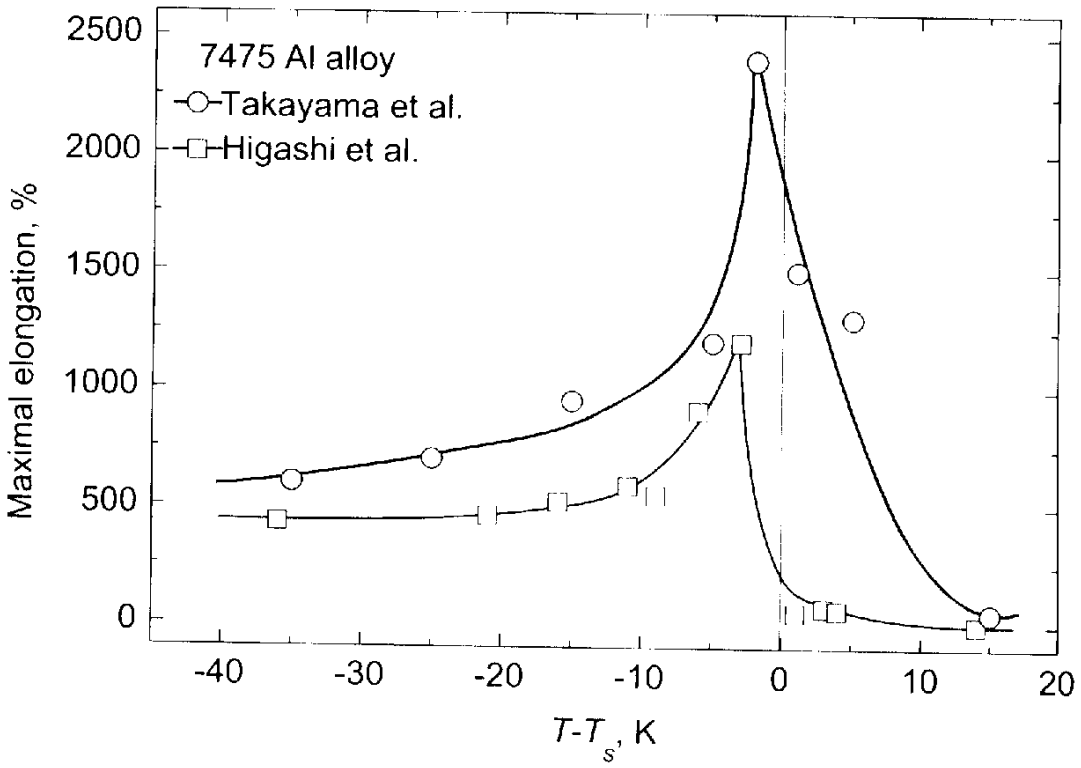

Figure 11. The temperature dependence of the maximal elongation of the 7475 Al–Zn–Mg alloy samples. T_s is the solidus temperature. Circles represent the data [50] and squares are taken from [51].

the GB segregation Z_Φ changes abruptly at a certain temperature (Fig. 10). Below this temperature the GB Bi concentration is constant and corresponds to a thin layer of pure Bi (GB phase). Above this temperature the GB segregation is lower than one monolayer of Bi and decreases gradually with increasing temperature according to the usual laws. These features indicate also the formation of a thin layer of a GB phase in the one-phase area of the bulk Cu–Bi phase diagram. The points of the abrupt change of the GB segregation form the GB solidus line in the bulk Cu–Bi phase diagram [22, 23, 39, 40]. GB segregation was measured with the aid of Auger electron spectroscopy (AES) on the GB fracture surfaces in samples broken *in situ* in the AES instrument. In other words, the multilayer GB segregation in Cu–Bi alloys leads to the increased *GB brittleness*. In [41] the GB energy was measured in Cu–Bi alloys using individual Σ19 GB in bicrystals with the aid of the GB thermal grooves. The thermal groove profile was obtained witt the aid of atomic force microscopy. The GB Bi segregation was measured simultaneously in the same conditions. The abrupt change of the segregation coincides with the *discontinuity of GB energy*. This fact demonstrates that the GB premelting (or prewetting) phase transition is of first order. The low-temperature measurements of resistivity temperature coefficient $d\rho/dT$ and residual resistivity ρ_0 at 4 K were performed in [40] using the Cu–Bi polycrystals annealed at high temperature and subsequently quenched. Both $d\rho/dT$ and ρ_0 demonstrate well pronounced break exactly at the same position where the sudden change of GB segregation was observed. In other words, the formation of GB layers of liquid-like phase leads to the measurable changes of *resistivity*.

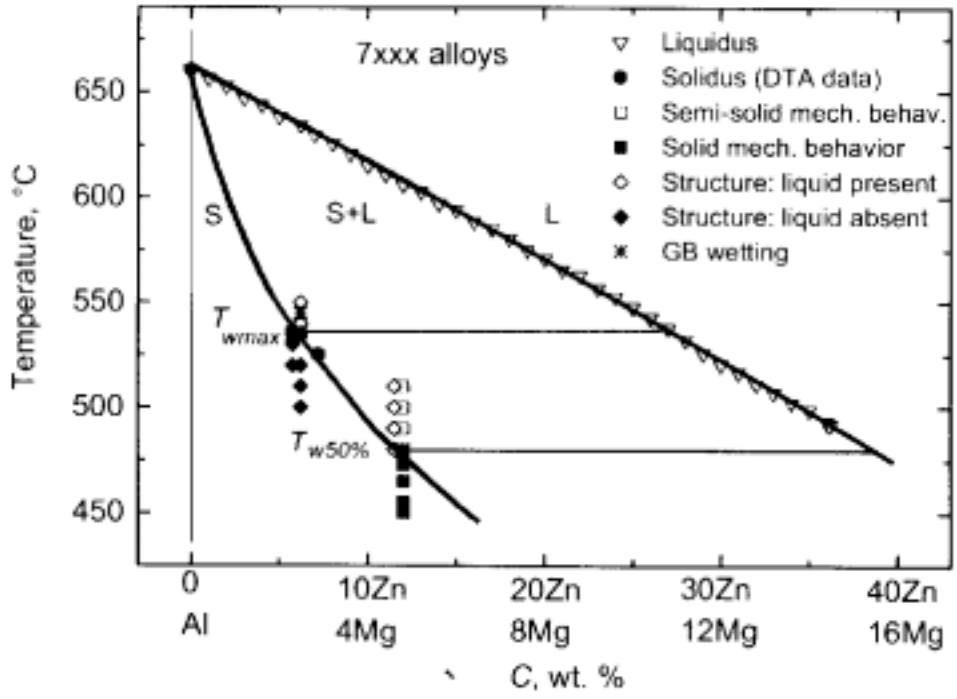

Figure 12. The phase diagram containing the GB wetting phase transition tie-lines constructed for the 7xxx Al–Zn–Mg alloys.

Superplastic forming of micrograined and nanostructured materials is a commercial, viable, manufacturing technology. One of the major drawbacks of conventional superplastic forming is that the phenomenon is only found at relatively low strain rates, typically about 10^{-4} to 10^{-3} s^{-1}. Recently, a number of studies have indicated that superplasticity of nanostructured materials can sometimes occur at extremely high strain rates (greater than 10^{-3} s^{-1} and up to 10^{2} s^{-1}). A specific example is a tensile elongation of over 1250% recorded at a strain rate of 10^{2} s^{-1} [42]. Thus far, this phenomenon, denoted as high-strain-rate superplasticity (HSRS), has been reported in several classes of materials, including metal alloys [42], metal-matrix composites [43–46] and mechanically-alloyed materials [47–49]. Despite these extensive experimental observations, the fundamental understanding of the factors leading to HSRS has not yet been arrived at. One very pertinent fact is that all of the materials that exhibit HSRS have a very fine grain size (~ 1 μm and less). Another is that the phenomenon is observed at rather high homologous matrix temperatures and very close to the matrix solidus temperature. In Fig. 11 the example is shown of HSRS for the 7475 Al–Zn–Mg alloy. The data are taken from independent works [50, 51] and reveal the very good reproducibility of the effect. Both temperature dependences have rather narrow maximum few degrees below the solidus temperature T_s. It is important to mention that the soludus temperature was measured by the differential thermal analysis (DTA) in the same works [50, 51]. The maximum elongation to failure reaches 1250 %. Below T_s the maximal elongation is about 500 %, above T_s the maximal elongation drops very quickly down to almost 0%.

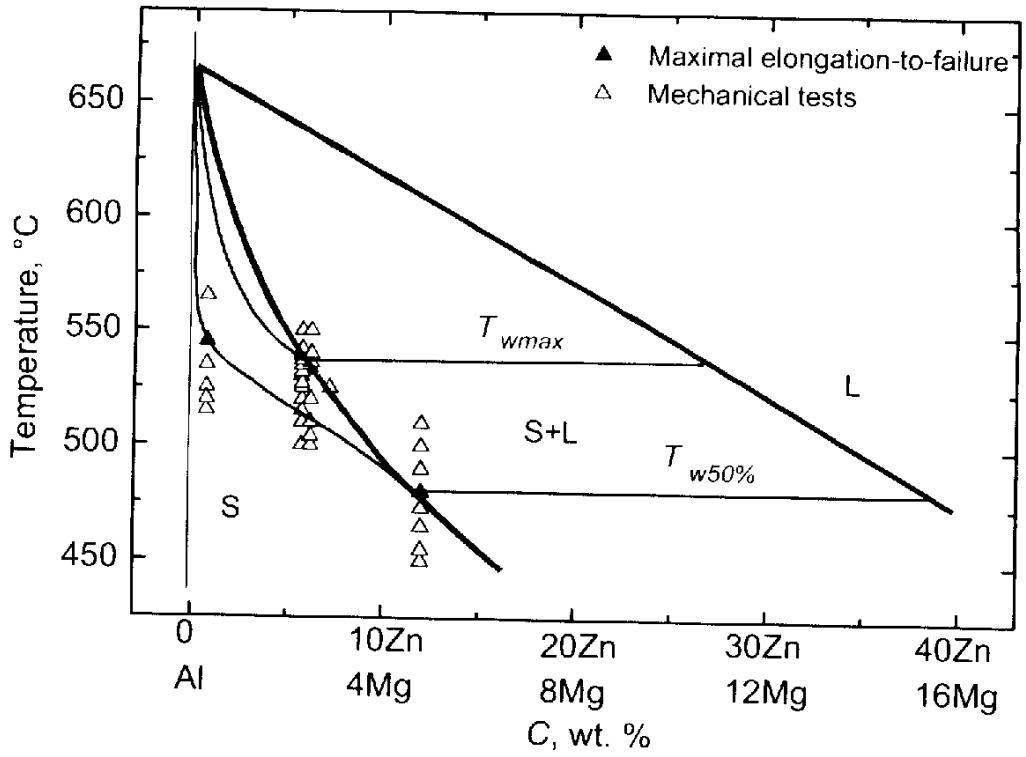

Figure 13. The phase diagram containing the GB wetting phase transition tie-lines and GB solidus lines constructed for the 7xxx Al–Zn–Mg alloys.

We suppose that the HSRS phenomenon can be explained using the ideas on the GB phase transitions in the two-phase *S+L* area and the solid solution area of the bulk phase diagrams. Using the data published in the literature, we constructed the lines of the GB wetting phase transition for the 7xxx Al–Zn–Mg alloys (Fig. 12). The liquidis line (thick solid line, open down triangles) have been cosntructed using the linear interpolation of liquidus lines for the binary Al Mg and Al–Zn phase diagrams [52]. Solidus line (thick solid line, full circles) has been drawn through the melting point for Al [52] and experimental points obtained using DTA for the 7xxx alloys [35, 50, 51, 53]. Open and full squares mark the solid and semi-solid mechanical behaviour, respectively [35]. Open and full diamonds mark the samples where the microstructural observations revealed the presence or absence of the liquid phase, respectively [35, 50, 51]. The analysis of the microstructures published in [35, 50, 51] permitted us to estimate the fraction of completely and partially wetted GBs (data marked by stars). These estimations allow to construct the GB wetting transition tie-lines (thin solid lines) for the T_{wmax} (above T_{wmax} all high-angle GBs in the polycrystal are completely wetted) [50, 51] and $T_{w50\%}$ (above $T_{w50\%}$ about 50% of the high-angle GBs in the polycrystal are completely wetted) [35].

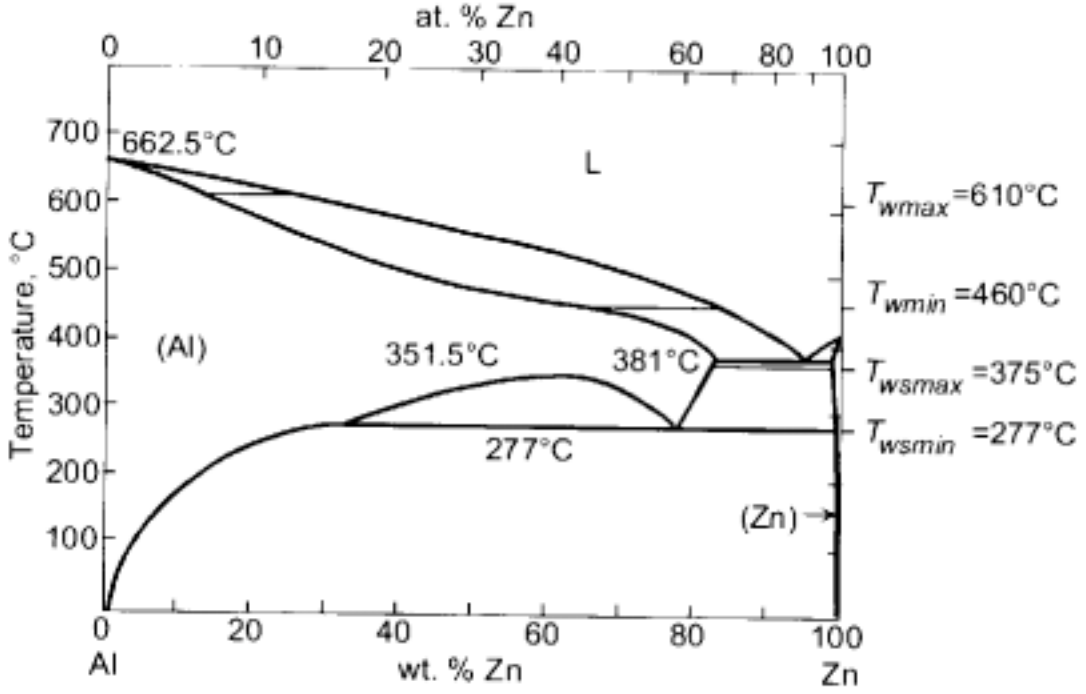

Figure 14. The Al–Zn phase diagram. Thick lines represent the bulk phase transitions. Thin lines are the tie-lines of the GB wetting phase transitions (T_{wmax} = 610°C and T_{wmin} = 460°C) and tie-lines of the GB covering («solid state wetting») phase transitions (T_{wsmax} = 375°C and T_{wsmin} = 277°C).

In the Fig. 12 the liquidus, solidus lines and GB wetting tie lines obtained in the Fig. 11 are repeated without experimental points. The data on mechanical tests (full and open up-triangles) are added [50, 53–55]. Full triangles mark the maximal elongation-to-failure obtained in the tests performed at different temperatures [50, 51, 54]. Full triangles lye either below the bulk solidus line or coincide with it. The temperature difference between temperature of the maximal elongation-to-failure and T_s decreases with increasing concentration of Mg and Zn. According to the thermodynamics, the tie lines of the GB wetting phase transition cannot finish at the intersection with the bulk solidus. They have to form the GB solidus line which continue in the solid solution area of the bulk phase diagram and finish in the melting point of the pure component. In the limiting case the degenerated GB solidus coincide with the bulk solidus. But in some systems it can extend into the solid solution area like it is shown in Fig. 4. In that case the layer of the liquid-like GB phase exist in the GBs between the GB and bulk solidus lines. We have shown above that the presence of such liquid-like layer in GB leads to the enhanced GB diffusivity, mobility and segregation of the second component [5, 11–17]. Such GB solidus lines are drawn also in Fig. 13 (thin solid lines). They continue the T_{wmax} and $T_{w50\%}$ GB wetting tie lines and finish in the melting point of Al. The GB solidus lines are drawn in such a way that the points of the maximal elongation-to-failure are between the GB and bulk solidus. Therefore, the enhanced plasticity of the nanograined polycrystals can be explained by the GB phase transition leading to the formation of the liquid-like layer on the GB in the narrow band of the solid solution area, just below the bulk solidus line. The phase diagrams similar to those shown in Figs 12 and 13 can be constructed using the published data on HSRS, DTA and

microscopy also for the 2xxx (Al–Zn–Mg) [45, 47–59, 51, 56–58], 5xxx (Al–Mg) [47, 51, 59, 60] and 6xxx (Al–Si–Mg) [59, 61–64] alloys. All authors studied the HSRS phenomenon mention that the physical reason of such a huge and reproducible increase of the palsticity is unknown. We suppose for the first time that the HSRS phenomenon can be explained by the existence of the equilibrium GB liquid-like layer close to the bulk solidus.

4. Grain Boundary Wetting (Covering) by Solid Phase

The situation illustrated in Fig. 1 can repeat in case if second phase (β) is not liquid but also solid. In other words, if in the phase α the GB energy $\sigma_{\alpha\alpha}$ is lower that the energy of two α/β solid/solid interfaces, the GB αα has to be substituted by the layer of the second solid phase β. Such process can be called the GB wetting (or covering) by solid phase. It is clear, that the kinetics of the equlibration processes in case GB wetting (or covering) by solid phase is much slower than in case of wetting by liquid phase. Our preliminary experiments with Al–95 wt.% Zn alloy demonstrate that after about 1 month of annealing the difference in the morphology of Al-rich phase precipitates (Al) at the (Zn)/(Zn) GBs in Zn-rich phase can be observed (Fig. 14). Namely, at high tempreratures just below the eutectic temperature in the Al–Zn system, more than 50% of (Zn)/(Zn) GBs are covered by continuous layer of the Al-rich phase. With decreasing temperature the portion of the (Zn)/(Zn) GBs covered by the (Al) layer decreased, and at the temperatures just below the eutectoid point all (Al) precipitates at the (Zn)/(Zn) GBs have the shape of isolated particles. Another examples of the GB covering phase transitions can be found by the analysis of the data published in the literature, for example, for Zr–Nb [65] or W–Cu systems [66–71].

5. Conclusions

The GB phase transitions can be observed both in two-phase and one-phase areas of bulk phase diagrams. In the two-phase $S+L$ area where solid and liquid phases are in equilibrium the GB wetting phase transition can take place at $T_{и}$. Above $T_{и}$ the GB disappears being substituted by two solid/liquid interfaces and the (macroscopically thick) layer of the liquid phase. The tie-lines of the GB wetting phase transition must have a continuation (GB solidus) in the one-phase S area of the bulk phase diagram. By intersection of GB solidus line the GB prewetting or premelting phase transition proceeds. Between the lines of GB and bulk solidus the grain boundary is substituted by two solid/liquid interfaces and the thin layer of the liquid-like phase. This liquid-like phase is stable in the GB and unstable in the bulk. The liquid-like phase is stabilized in GB due to the energy gain which appears as a result of

substitution of GB by two solid/liquid interfaces. The GB wetting and prewetting (premelting) phase transitions observed up-to-date are of first order. If the GB energy is higher than the energy of two solid/solid interfaces, the GB solid state wetting (covering) phase transition can occur in a two-phase S_1+S_2 area of the phase diagram.

6. Acknowledgements

The financial support of Russian Foundation for Basic Research and the Government of the Moscow district (contracts 01-02-97039 and 01-02-16473), Deutsche Forschungsgemein-schaft (contracts Gu 258/12-1 and Ba-1768/1-2), Copernicus program of EU (contract ICA2-CT-2001-10008) and the German Federal Ministry for Education and Research (contract WTZ RUS 00/209) is acknowledged.

7. References

1. Langdon, T.G., Watanabe, T., Wadsworth, J., Mayo, M.J., Nutt, S.R., and Kassner, M. E. (1993) Future research directions for interface engineering in high-temperature plasticity, *Mater. Sci. Eng. A* **166**, 237.
2. Straumal, B.B. and Gust, W. (1996) Lines of grain boundary phase transitions on the bulk phase diagrams, *Mater. Sci. Forum* **207–209**, 59-68.
3. Straumal, B., Molodov, D., and Gust, W. (1994) Tie lines of the grain boundary wetting phase transition in the Al–Sn system, *J. Phase Equilibria* **15**, 386-391.
4. Straumal, B., Muschik, T., Gust, W., and Predel, B. (1992) The wetting transition in high and low energy grain boundaries in the Cu(In) system, *Acta metall. mater.* **40**, 939-945.
5. Chang, L.-S., Rabkin, E., Straumal, B.B., Hofmann, S., Baretzky, B., and Gust, W. (1998) Grain boundary segregation in the Cu–Bi system, *Defect Diff. Forum* **156**, 135-146.
6. Straumal, B., Semenov, V., Glebovsky, V., and Gust, W. (1997) Grain boundary wetting phase transitions in the Mo–Ni system. *Defect Diff. Forum* **143–147**, 1517-1522.
7. Straumal, B.B., Gust, W., and Watanabe, T. (1999) Tie lines of the grain boundary wetting phase transition in the Zn-rich part of the Zn–Sn phase diagram, *Mater. Sci. Forum* **294–296**, 411-414.
8. Ernst, F., Finnis, M.W., Koch, A., Schmidt, C., Straumal, B., and Gust, W. (1996) Structure and energy of twin boundaries in copper, *Z. Metallk.* **87**, 911-922.
9. Straumal, B.B. and Shvindlerman, L.S. (1985) Regions of existence of special and non-special grain boundaries, *Acta metall.* **33**, 1735-1749.
10. Maksimova, E.L., Shvindlerman, L.S., and Straumal, B.B. (1988) Transformation of Σ17 special tilt boundaries to general boundaries in tin, *Acta metall.* **36**, 1573-1583.
11. Cahn, J.W. (1977) Wetting transitions on surface, *J. Chem. Phys.* **66**, 3667-3679.
12. Dietrich, S. (1988) Wetting transitions in interfaces, in C. Domb and J.H. Lebowitz (eds.), *Phase Transitions and Critical Phenomena*, 12, Academic Press, London, pp. 2-218.
13. Jasnov, D. (1984) Phase transitions on surfaces, *Rep. Prog. Phys.* **47**, 1059-1070.
14. de Gennes, G. (1985) Wetting: statics and dynamics, *Rev. Mod. Phys.* **57**, 827-863.
15. Kellay, H., Bonn, D., and Meunier, J. (1993) Prewetting in a binary liquid mixture, *Phys. Rev. Lett.* **71**, 2607-2610.
16. Schmidt, J.W. and Moldover, M.R. (1983) First-order wetting transition at a liquid-vapor interface, *J. Chem. Phys.* **79**, 379-387.
17. Eustatopoulos, N., Coudurier, L., Joud, J.C., and Desre, P. (1976) Solid-liquid interface tension of Al–Sn, Al–In and Al–Sn–In systems, *J. Crystal Growth* **33**, 105-115.
18. Straumal, B., Gust, W., and Molodov, D. (1995) Wetting transition on the grain boundaries in Al contacting with Sn-rich melt, *Interface Sci.* **3**, 127-132.
19. Straumal, B., Molodov, D., and Gust, W. (1996) Grain boundary wetting phase transitions in the Al–Sn

and Al–Pb–Sn systems, *Mater. Sci. Forum* **207–209**, 437-440.
20. Straumal, B., Risser, S., Sursaeva, V., Chenal, B., and Gust, W. (1995) Grain growth and grain boundary wetting transitions in the Al–Ga and Al–Sn–Ga alloys of high purity, *J. Physique* **IV 5-C7**, 233-241.
21. Molodov, D.A., Czubayko, U., Gottstein, G., Shvindlerman, L.S., Straumal, B.B., and Gust, W. (1995) Acceleration of grain boundary motion in Al by small additions of Ga, *Phil. Mag. Lett.* **72**, 361-368.
22. Chang, L.-S., Straumal, B.B., Rabkin, E., Gust, W., and Sommer, F. (1997) The solidus line of the Cu–Bi phase diagram, *J. Phase Equilibria* **18**, 128-135.
23. Chang, L.-S., Rabkin, E., Straumal, B., Lejcek, P., Hofmann, S., and Gust, W. (1997) Temperature dependence of the grain boundary segregation of Bi in Cu polycrystals, *Scripta mater.* **37**, 729-735.
24. Rabkin E.I., Semenov, V.N., Shvindlerman, L.S., and Straumal, B.B. (1991) Penetration of tin and zinc along tilt grain boundaries 43°[100] in Fe–5at.%Si alloy: Premelting phase transition? *Acta metall. mater.* **39**, 627-639.
25. Noskovich, O.I., Rabkin, E.I., Semenov, V.N., Shvindlerman, L.S., and Straumal, B.B. (1991) Wetting and premelting phase transitions in 38°[100] tilt grain boundaries in (Fe–12 at. % Si) Zn alloy in the vicinity of the A2–B2 bulk ordering in Fe–12 at. % Si alloy. *Acta metal. mater.* **39**, 3091-3098.
26. Straumal, B.B., Noskovich, O.I., Semenov, V.N., Shvindlerman, L.S., Gust, W., and Predel, B. (1992) Premelting transition on 38°<100> tilt grain boundaries in (Fe–10 at. % Si) Zn alloys, *Acta metall. mater.* **40**, 795-801.
27. Straumal, B., Rabkin, E., Lojkowski, W., Gust, W., and Shvindlerman, L.S. (1997) Pressure influence on the grain boundary wetting phase transition in Fe–Si alloys, *Acta mater.* **45**, 1931-1940.
28. Rabkin, E., Weygand, D., Straumal, B., Semenov, V., Gust, W., and Brèchet, Y. (1996) Liquid film migration in a Mo(Ni) bicrystal, *Phil. Mag. Lett.* **73**, 187-193.
29. Glebovsky, V.G., Straumal, B.B., Semenov, V.N., Sursaeva, V.G., and Gust, W. (1994) Grain boundary penetration of a Ni-rich melt in tungsten polycrystals, *High Temp. Mater. Proc.* **13**, 67-73.
30. Flemings, M.C. (1991) Behavior of metal alloys in the semisolid state, *Metall. Trans. A* **22**, 957-981.
31. Kumar, P., Martin, C.L., and Brown, S. (1993) Shear strain rate thickening flow behaviour of semisolid slurries, *Metall. Trans. A* **24**, 1107-1116.
32. Chen, C.P. and Tsao, C.-Y.A. (1997) Semi-solid deformation of non-dendritic structures .1. Phenomenological behavior, *Acta mater.* **45**, 1955-1968.
33. Roth, M.C., Weatherly, G.C., and Miller, W.A. (1980) The temperature dependence of the mechanical properties of aluminum alloys containing low-melting-point inclusions, *Acta metall.* **28**, 841-853.
34. Vaandrager, B.L. and Pharr, G.M. (1989) Compressive creep of copper containing a liquid bismuth intergranular phase, *Acta metall.* **37**, 1057-1066.
35. Baudelet, B., Dang, M.C. and, Bordeaux, F. (1995) Mechanical behaviour of an aluminium alloy with fusible grain boundaries, *Scripta Metall. Mater.* **32**, 707-712.
36. Iwasaki, H., Mori, T., Mabuchi, M., and Higashi, K. (1998) Shear deformation behavior of Al–5% Mg in a semi-solid state, *Acta mater.* **46**, 6351-6360.
37. Pharr, G.M., Godavarti, P.S., and Vaandrager, B.L. (1989) Effects of wetting on the compression creep-behavior of metals containing low melting intergarnular phases, *J. Mater. Sci.* **24**, 784-792.
38. Cahn, J.W. (1982) Transitions and phase equilibria among grain boundary structures, *J. Phys.Colloq.* **43-C6**, 199-213.
39. Chang, L.-S., Rabkin, E., Straumal, B.B., Baretzky, B., and Gust, W. (1999) Thermodynamic aspects of the grain boundary segregation in Cu(Bi) alloys, *Acta mater.* **47**, 4041-4046.
40. Straumal, B., Sluchanko, N.E., and Gust, W. (2001) Influence of the grain boundary phase transitions on the properties of Cu–Bi polycrystals, *Def. Diff. Forum* **188–190**, 185-194.
41. Schölhammer, J., Baretzky, B., Gust, W., Mittemeijer, E., and Straumal, B. (2001) Grain boundary grooving as an indicator of grain boundary phase transformations, *Interf. Sci.* **9**, 43-53.
42. Higashi, K., Tanimura, S., and Ito, T. (1990) Superplastic behaviour at high-strain rates in a particulate 6061 aluminium composites, *MRS Proc.* **196**, 385-390.
43. Imai, T., Mabuchi, M., Tozawa, Y., and Yamada, M. (1990) Superplasticity in beta-silicon nitride whisker reinforced 2124 aluminum composite, *J. Mater. Sci. Lett.* **2**, 255-257.
44. Mabuchi, M. and Imai, T. (1990) Superplasticity of Si_3N_4 whisker reinforced 6061 aluminum at high strain rate, *J. Mater. Sci. Lett.* **9**, 761-762.
45. Nieh, T.G., Henshall, C.A., and Wadsworth, J. (1984) Superplasticity at high strain rates in a SiC whisker reinforced Al alloy, *Scripta Metall.* **18**, 1405-1408.
46. Mabuchi, M., Higashi, K., Okada, Y., Tanimura, S., Imai, T., and Kubo, K. (1991) Superplastic behaviour at high-strain rates in a particulate Si_3N_4 6061 aluminium composite, *Scripta Metall.* **25**, 2003.

47. Nieh, T.G., Gilman, P.S., and Wadsworth, J. (1985) Extended ductility at high strain rates in a mechanically alloyed aluminum alloy, *Scripta Metall.* **19**, 1375-1378.
48. Bieler, T.R., Nieh, T.G., Wadsworth, J., and Mukherjee, A.K. (1988) Superplastic-like behaviour at high strain rates in mechanically alloyed aluminum, *Scripta Metall.* **22**, 81-86.
49. Higashi, K., Okada, Y., Mukai, T., and Tanimura, S. (1991) Positive exponent strain-rate superplasticity in mechanically alloyed aluminum IN9021, *Scripta Metall.* **25**, 2053-2057.
50. Takayama, Y., Tozawa, T., and Kato, H. (1999) Superplasticity and thickness of liquid phase in the vicinity of solidus temperature in a 7475 aluminum alloy, *Acta mater.* **47**, 1263-1270.
51. Higashi, K., Nieh, T.G., Mabuchi, M., and Wadsworth, J. (1995) Effect of liquid phases on the tensile elongation of superplastic aluminum alloys and composites, *Scripta metall. mater.* **32**, 1079-1084.
52. Apykhtina, I., Bokstein, B., Khusnutdinova, A., Peteline, A., and Rakov, S. (2001) Kinetics of diffusion-controlled grooving in solid-liquid systems, *Def. Diff. Forum* **194–199**, 1331-1336.
53. Imai, T., Mabuchi, M., Tozawa, Y., Murase, Y., and Kusui, J. (1990) in R.B. Bhagat. et al. (eds.), *Metal & Ceramic Matrix Composites: Processing, Modeling & Mechanical Behavior*, TMS-AIME, Warrendale, Pennsylvania, pp. 235-239.
54. Mabuchi, M., Higashi, K., Imai, T., and Kubo, K. (1991) Superplastic-like behavior in as-extruded Al–Zn–Mg alloy matrix composites reinforced with Si_3N_4 whiskers, *Scripta Metall.* **25**, 1675-1680.
55. Furushiro, N., Hori, S., and Miyake, Y. (1991) in S. Hori et al., (eds.) *Proc. Int. Conf. Superplast. Adv. Mats (ICSAM-91)*, Jap. Soc. Res. Superplast., Tokyo, pp. 557-562.
56. Mabuchi, M., Higashi, K., and Langdon, T. (1994) An investigation of the role of a liquid-phase in Al Cu Mg metal-matrix composites exhibiting high-strain rate suparplasticity, *Acta metall. mater.* **42**, 1739-1745.
57. Mabuchi, M., Higashi, K., Wada, S., and Tanimura, S. (1992) Superplastic behavior in as-extruded Al Cu Mg alloy matrix composite reinforced with 20 vol. % Si_3N_4 partciculates, *Scripta Metall.* **26**, 1269-1274.
58. Nieh, T.G. and Wadsworth, J. (1993) *Scripta Metall.* **28**, 1119.
59. Mabuchi, M., Higashi, K., Inoue, K., and Tanimura, S. (1992) Experimental investigation of superplastic behavior in a 20 vol. % Si_3N_4P/5052 aluminium composite, *Scripta Metall.* **26**, 1839.
60. Koike, J., Mabuchi, M., and Higashi, K. (1995) In-situ observation of partial melting in superplastic aluminium-alloy composites at high-temparatures, *Acta metall. mater.* **43**, 199-206.
61. Mabuchi, M., Higashi, K., Okada, Y., Tanimura, S., Imai, T., and Kubo, K. (1991) Very high strain-rate superplasticity in a particulate Si_3N_4/6061 aluminium composite, *Scripta Metall.* **25**, 2517-2522.
62. Hikosaka, T., Imai, T., Nieh, T.G., and Wadsworth, J. (1994) High-strain rate superplasticity of a SiC particulate-reinforced aluminium alloy composite by a vortex method, *Scripta Metall.* **31**, 1181-1186.
63. Grishaber, R.B., Mishra, R.S., and Mukherjee, A.K. (1996) Effect of testing environment on intergranular microsuperplasticity in an aluminum MMC, *Mat. Sci. & Eng. A* **220**, 78-84.
64. Nieh, T.G., Lesuer, D.R., and Syn, C.K. (1995) Tensile and fatigue properties of a 25 vol. % SiC SIC particulate-reinforced 6090-Al composite at 300°C, *Scripta Metall. Mater.* **32**, 707-712.
65. Iribarren, M.J., Agüero, O.E., and Dyment, F. (2001) Co-diffusion along the alpha/beta interphase boundaries of a Zr 2.5% Nb alloy, *Def. Diff. Forum.* **194–199**, 1211-1216.
66. Geguzin, Ya.E. (1984) *Physics of Sintering*, 2nd edition. Nauka, Moscow (in Russian).
67. Eremenko, V.N., Naidich, Yu.V., and Lavrinenko, I.A. (1968) *Sintering in the Presence of Liquid Phase*. Naukova dumka, Kiev (in Russian).
68. Panichkina, V.V., Sirotjuk, M.M., and Skorokhod, V.V. (1982) Liquid-phase sintering of higly disperced W Cu mixtures, *Poroshk. Metall.* **6**, 21 (in Russian).
69. Skorokhod, V.V., Panichkina, V.V., and Prokushev, N.K. (1986) Microstructural inhomogeneity and localization of densification during liquid-phase sintering of W–Cu powder mixtures *Poroshk. Metall.* **8**, 14 (in Russian).
70. Skorokhod, V.V., Solonin, Yu.M., Filippov, N.I., and Poshin, A.N. (1983) Sintering of W–Cu mixtures *Poroshk. Metall.* **9**, 9 (in Russian).
71. Huppmann, W.J. and Riegger, H. (1975) Modeling of rearrangement processes in liquid phase sintering, *Acta metall.* **23**, 965-971.